

PAPER

## The fixed oxide trap modelling during isothermal and isochronal annealing of irradiated RADFETs

To cite this article: Goran S Risti *et al* 2012 *J. Phys. D: Appl. Phys.* **45** 305101

View the [article online](#) for updates and enhancements.

### Related content

- [Thermal and UV annealing of irradiated pMOS dosimetric transistors](#)  
Goran S Risti
- [Topical Review](#)  
Goran S Ristic
- [Interface and oxide state behaviors of commercial n-channel power MOSFETs](#)  
Goran S Risti and Nikola D Vasovi

### Recent citations

- [Improvement of radiation response of SiC MOSFETs under high temperature and humidity conditions](#)  
Akinori Takeyama *et al*
- [P. Goncalves \*et al\*](#)



**IOP | ebooks™**

Bringing you innovative digital publishing with leading voices to create your essential collection of books in STEM research.

Start exploring the collection - download the first chapter of every title for free.

# The fixed oxide trap modelling during isothermal and isochronal annealing of irradiated RADFETs

Goran S Ristić<sup>1</sup>, Nikola D Vasović<sup>1</sup> and Aleksandar B Jakšić<sup>2</sup>

<sup>1</sup> Applied Physics Laboratory, Faculty of Electronic Engineering, University of Niš, PO Box 73, 18001 Niš, Serbia

<sup>2</sup> Tyndall National Institute, Lee Maltings, Cork, Ireland

E-mail: [goran.ristic@elfak.ni.ac.rs](mailto:goran.ristic@elfak.ni.ac.rs)

Received 6 December 2011, in final form 16 May 2012

Published 10 July 2012

Online at [stacks.iop.org/JPhysD/45/305101](http://stacks.iop.org/JPhysD/45/305101)

## Abstract

The density of fixed traps (FTs),  $\Delta N_{\text{ft}}$  ( $\text{cm}^{-2}$ ), during isothermal annealing of irradiated radiation-sensitive field-effect transistors (RADFETs) from room temperature to 200 °C has been modelled. The modelling has shown that a simple, two-defect model (2DM), containing two defect types: one defect type for positively charged FTs (PCFTs), and another for negatively charged FTs (NCFTs), is applicable for the temperatures up to 100 °C. However, the three-defect model (3DM), which includes additional PCFT type, should be used for temperatures from 100 to 200 °C. The models describing the behaviour of NCFTs during isothermal annealing have also been analysed. The activation energies of  $E_{\text{a}1}^+ = 0.27$  eV,  $E_{\text{a}2}^+ = 0.45$  eV and  $E_{\text{a}}^- = 0.25$  eV, for two PCFT types and one NCFT type, respectively, have been found. In addition, isochronal unannealed curves have been well fitted using logistic function. The modelling of isochronal annealing has also shown that one PCFT type up to 100 °C, and two PCFT types for 100–200 °C, respectively, are active, and additional defect(s) should be included for the temperatures higher than 200 °C. The isochronal annealing, which is significantly less time consuming than isothermal annealing, could be very good tool for the revealing of defects created by various stress types.

## 1. Introduction

The dosimeters based on dosimetric p-channel metal-oxide-semiconductor field-effect transistors (pMOSFETs), also called radiation-sensitive FETs (RADFETs) or pMOS dosimeter, are very attractive for applications in space [1–4], nuclear facilities [5–10] and radiotherapy clinics [11–15].

During irradiation and annealing of RADFETs, only the threshold voltage,  $V_{\text{T}}$ , is usually investigated. In that way, RADFET has been considered as a 'black box' that gives an electrical output ( $V_{\text{T}}$ ) as a response to the input (ionizing radiation or high temperature). However, from a practical point of view, it is essential to know the behaviour of the created defects, as that would allow the modification of RADFET manufacturing process in order to improve their sensitivity to radiation, fading (spontaneous room-temperature annealing) and thermal annealing, thus obtaining desired device performances and enabling reuse of dosimeters.

Thermal annealing at the constant temperature (isothermal annealing) of irradiated MOSFETs has attracted researchers for years [16–21]. It is a good tool for the revealing of the nature of the defects induced in MOSFETs by ionizing radiation (radiation defects). The other kind of thermal annealing of radiation defects is isochronal annealing [21–25], i.e. thermal annealing with temperature increasing in constant steps, with a fixed time period for each temperature.

In this paper, the modelling of fixed oxide trap density,  $\Delta N_{\text{ft}}$ , induced by ionizing radiation, during isothermal and isochronal annealing of RADFET (pMOS) dosimeters has been performed. The modelling of isothermal annealing was performed using the fixed trap (FT) annealing reactions and biomolecular theory. The equations obtained by the two-defect model (2DM) and three-defect model (3DM) fit the experimental results of isothermal annealing of  $\Delta N_{\text{ft}}$  very well. The isochronal annealing of  $\Delta N_{\text{ft}}$  was modelled using semi-empirical logistic function, and a procedure for activation energy determination was discussed.

## 2. Experimental details

The experimental samples were Al-gate dosimetric pMOS transistors (RADFETs), manufactured by Tyndall National Institute, Cork, Ireland. The transistors had  $t_{ox} = 100$  nm thick gate oxide, grown at  $1000^\circ\text{C}$  in dry oxygen, and annealed for 15 min at  $1000^\circ\text{C}$  in nitrogen. The post-metallization anneal was performed at  $440^\circ\text{C}$  in forming gas for 60 min [26]. The RADFET chip contains four individual transistors. Two transistors have a channel width of  $W = 300\ \mu\text{m}$ , and a channel length of  $L = 50\ \mu\text{m}$  (300/50 type), and another two transistors are of 690/15 type. If it is not noted, the results of 300/50 transistors are presented; the results for 690/15 samples are noted.

The irradiation was performed in the Metrology Laboratory of Vinča Institute of Nuclear Science, Belgrade. The experimental samples were irradiated at room temperature without gate bias,  $V_{Gi} = 0$  V (all pins were grounded), using the  $^{60}\text{Co}$  source up to the absorbed dose of  $D = 1800$  Gy(Si) at the absorbed dose rate of  $\dot{D} = 0.055$  Gy(Si)  $\text{s}^{-1}$ . The irradiation exposure time was 9 h at the distance from the source to the samples of 107 mm.

After irradiation, the samples were divided into two groups. The transistors from the first group were isothermally annealed at room temperature, 60, 100, 150 and  $200^\circ\text{C}$ . During isothermal annealing, at the specific points, the transistors are cooled-down and transfer characteristics were measured at room temperature (figure 1(a)).  $t_{up}$  is a time of sampling temperature heating, and  $t_{down}$  is a time of sampling cooling. In our case, the furnace (temperature chamber) is used, and the devices are removed from and returned to the furnace, so that  $t_{down}$  is the period from the moment when the devices are taken out of the furnace to the moment when they are cooled to room temperature, and  $t_{up}$  is period from the moment when the devices are put in the furnace to the moment when they are heated to the given temperature. It could be expected that  $t_{down}$  and  $t_{up}$  are very short periods of time, because the electric fan is used for the device cooling, but the furnace was continuously kept at the given temperature.

$t_{anneal1}, t_{anneal2}, t_{anneal3} \dots$ , i.e.  $\Delta t_1 = t_{anneal1}, \Delta t_2 = t_{anneal2}, \Delta t_3 = t_{anneal3}$ , etc are the annealing times, but  $t_{m1}, t_{m2}$ , etc, are the measurement times and they are short (in average, about 1 minute) and approximately the same ( $t_{m1} \approx t_{m2} \approx \dots \approx 1$  min.).

The transistors from the second group were isochronally annealed from 60 to  $310^\circ\text{C}$ . The annealing cycles are shown in figure 1(b) and all measurements were performed at room temperature. Similarly with the isochronal annealing, the furnace was used and devices were taken out of the furnace for the measurements, and put in the furnace for the annealing. The temperature raised in the constant temperature steps,  $\Delta T$ , and the annealing interval,  $\Delta t$  ( $\equiv t_{anneal}$ ), at each temperature was the same.  $t'_{m1}, t'_{m2}, \dots$ , are the measurement times that are short and approximately the same ( $t'_{m1} \approx t'_{m2} \approx \dots \approx 1$  min.).

The isothermal and isochronal annealing were performed without gate bias ( $V_{Ga} = 0$  V; all pins grounded) using the Heraeus HEP2 system of temperature chambers.  $V_{Gi,a} = 0$  V corresponds to a small positive electric field in the oxide

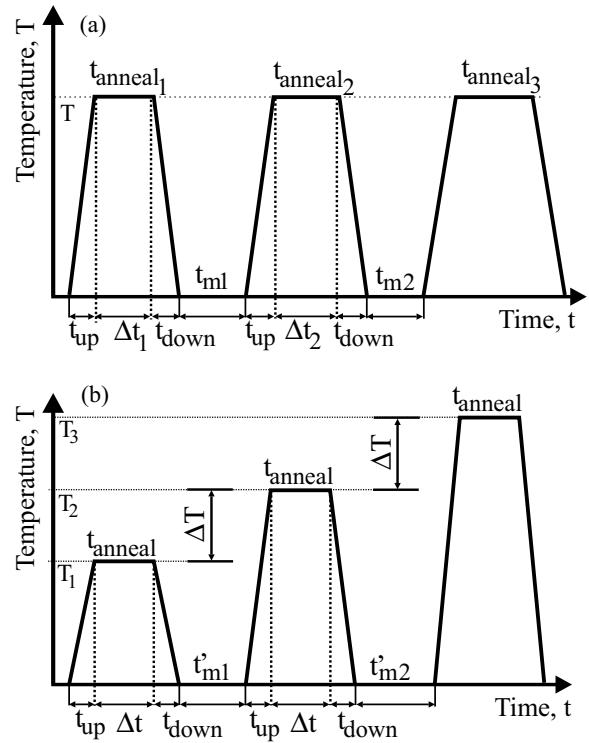


**Figure 1.** Temperature profiles of (a) isothermal, and (b) isochronal annealing ( $T_{i+1} = T_i + \Delta T$ ).

( $E_{wf}$ ) due to a work function difference between Al-gate and n-type silicon substrate of  $V_{wf} \approx 0.33$  V ( $E_{wf} = V_{wf}/t_{ox} = 3.3$  V  $\mu\text{m}^{-1}$ ).

The transistor threshold voltage before irradiation,  $V_{T0}$ , as well as during irradiation and annealing,  $V_T$ , were determined by the transfer characteristics in saturation, i.e. as the intersection between  $V_G$ -axis and the extrapolated linear region of the  $(I_D)^{1/2} - V_G$  curves [27]. A low current dual-channel source meter unit (SMU) model 2636A Keithley connected to the test fixture is used for the measurements of transfer characteristics. Using the channel #A of Keithley 2636A SMU, the dc voltage was applied to the transistor gate in the steps of 0.05 V, while the channel #B of Keithley 2636A was used for the drain biasing with a constant voltage of  $V_D = 15$  V and the drain-source current  $I_D$  measurements. The source and bulk were grounded, and  $I_D$  was measured and recorded in the range from  $10^{-11}$  to  $10^{-3}$  A.

The midgap-subthreshold (MG) technique [28] for determination of the densities of FTs and switching traps (STs) has been used. The FTs represent the traps created in the gate oxide, and STs represent the traps created near and at the oxide/substrate ( $\text{SiO}_2/\text{Si}$ ) interface. The STs created in the oxide, near  $\text{SiO}_2/\text{Si}$  interface, are called the slow switching (border) traps (SSTs), while the STs created at this interface are called the fast switching (true interface) traps (FSTs). FTs represent traps in the gate oxide that do not exchange the carriers from the channel, but the SSTs and FSTs, making the STs, represent the traps that do exchange (communicate with) the carriers from the channel within the time frame of electrical MG measurements [27]. FTs and SSTs are known as the oxide trapped charge, and FSTs as the interface traps.

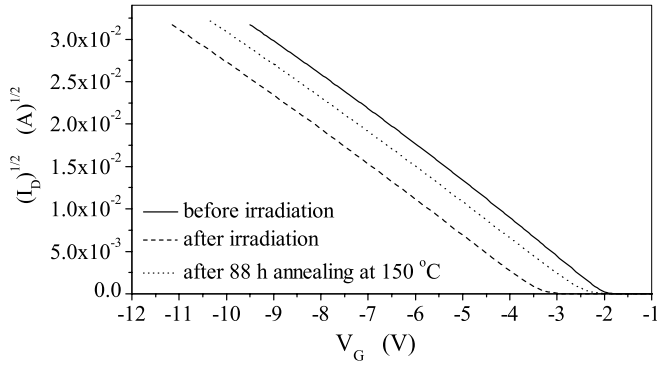


Figure 2. Transfer characteristics of RADFETs.

The contribution of FTs,  $\Delta V_{ft}$ , and STs,  $\Delta V_{st}$ , to the net threshold voltage shift  $\Delta V_T$  is

$$\Delta V_T = \Delta V_{ft} + \Delta V_{st}. \quad (1)$$

$\Delta V_T$  increases with increase in both FTs and STs in the pMOS transistors.

The areal density of FTs,  $\Delta N_{ft}$  ( $\text{cm}^{-2}$ ), and the areal density of STs,  $\Delta N_{st}$  ( $\text{cm}^{-2}$ ), after irradiation/annealing could be determined as [28]

$$\Delta N_{ft} = \pm \frac{C_{ox}}{q} \Delta V_{ft}, \quad \Delta N_{st} = \frac{C_{ox}}{q} \Delta V_{st}, \quad (2)$$

where  $C_{ox}$  is oxide capacitance per unit area, and  $q$  absolute value of electron charge. The signs '+' and '-' are for p-channel and n-channel MOSFETs, respectively. Figure 2 shows the  $\sqrt{I_D} = f(V_G)$  of transfer characteristics and figure 3 shows these transfer characteristics in lin-log scale (so-called subthreshold characteristics) of RADFETs before and after irradiation, as well as after isothermal annealing of 88 h at  $t = 150^\circ\text{C}$ . Only the parts of subthreshold characteristics, important for MG characteristics, are shown.

The  $\Delta N_{ft}$  and  $\Delta N_{st}$ (MG) were used in this study as they reflected the electrical response of the traps. Namely, since the electrical measurement technique is employed, then  $\Delta N_{ft}$  and  $\Delta N_{st}$ (MG) are more suitable than more commonly used quantities that imply the physical location of the traps: density of oxide traps (oxide trapped charge density)  $\Delta N_{ot}$  and interface traps density  $\Delta N_{it}$ . The correlations between these quantities are  $\Delta N_{ot} = \Delta N_{ft} + \Delta N_{sst}$  and  $\Delta N_{it} = \Delta N_{st} - \Delta N_{sst} = \Delta N_{fst}$ , where  $\Delta N_{sst}$  is the SST density, and  $\Delta N_{fst}$  is the FST density. Since the electrical techniques were used, it was not possible to reveal the defect types, but only the defect densities.

### 3. Results and discussion

#### 3.1. Isothermal annealing

Figure 4 shows  $\Delta N_{ft}$  and  $\Delta N_{st}$  during isothermal annealing at various temperatures ( $V_{Ga} = 0\text{ V}$ ), and for all temperatures  $\Delta N_{ft}$  decreases with annealing time. The changes of  $\Delta N_{st}$  are not significant, indicating that the annealing has not occurred (except for  $200^\circ\text{C}$ ).

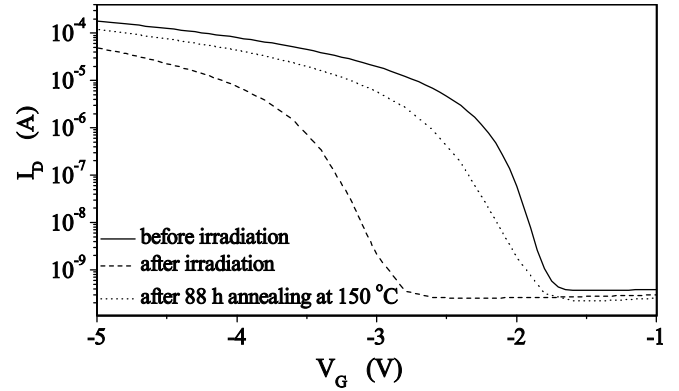


Figure 3. Subthreshold characteristics, representing transfer characteristics in semi-logarithm scale from figure 2 for  $V_G > -5\text{ V}$ .

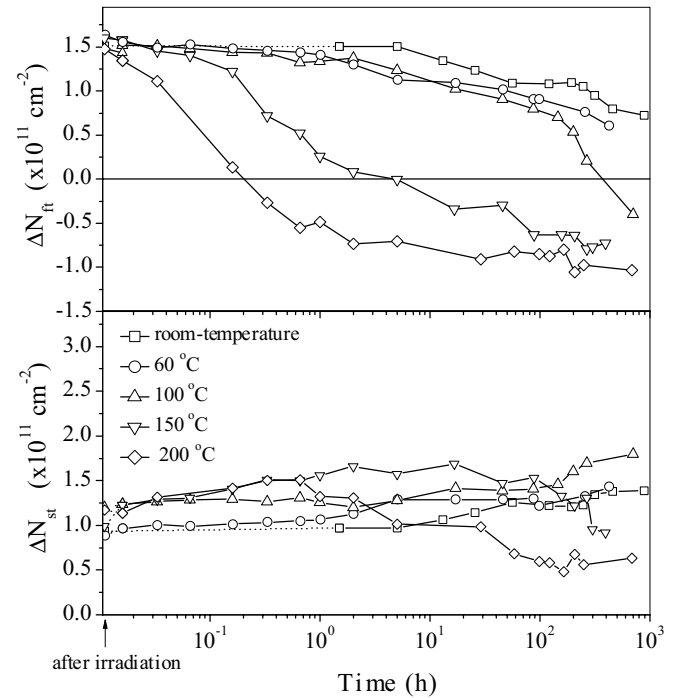
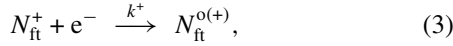


Figure 4. Isothermal annealing of RADFETs with  $V_{Ga} = 0\text{ V}$ .

**3.1.1. Two-defect model (2DM).** Since the values of  $\Delta N_{ft}$  turns negative for the three highest temperatures, it could be supposed that  $\Delta N_{ft}$  contains two parts, a part of positively charged FTs (PCFTs) and a part of negatively charged FTs (NCFTs). Namely,  $\Delta N_{ft}$  obtains negative values during isothermal annealing at 100, 150 and  $200^\circ\text{C}$  as a consequence of domination of NCFTs over PCFTs. Otherwise, FTs are mostly positively charged, since a lot of holes released by radiation are captured, creating the PCFTs [29]. However, some FTs are negatively charged (NCFTs), and they are formed by amphoteric NCFT precursors that capture the electrons released by radiation [21, 27].

The density of FTs ( $\Delta N_{ft}$ ) has been initially modelled using the 2DM: one defect type represents the PCFT, and another type represents the NCFT. During the isothermal annealing, PCFT density,  $\Delta N_{ft}^+(t)$ , decreases as a consequence of the neutralization and/or compensation of PCFTs by the electrons that tunnel from the substrate. The reaction of

PCFT neutralization and/or compensation during isothermal annealing is [21]



where  $N_{\text{ft}}^+$  denotes the PCFT,  $e^-$  denotes the tunnelling electron,  $k^+$  is the reaction rate constant and  $N_{\text{ft}}^{o(+)}$  denotes annealed PCFT.

Using reaction (3) and bimolecular theory [30–32], the reaction rate  $R_1$  could be obtained [21]:

$$R_1 \equiv -\frac{d[N_{\text{ft}}^+]}{dt} = k^+[N_{\text{ft}}^+][e^-]. \quad (4)$$

$[N_{\text{ft}}^+]$  is the density of PCFTs, and  $[e^-]$  is the concentration of incoming electrons. The minus sign indicates the  $[N_{\text{ft}}^+]$  decreasing with time as the reaction proceeds.

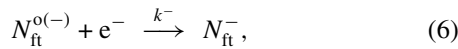
The solving of differential equation (4) gives the following equation for the PCFT density, obtained by the MG technique, decreasing with annealing time [21]:

$$\Delta N_{\text{ft}}^+(t) = \Delta N_{\text{ft}}^+(0) \cdot e^{-t/\tau^+}. \quad (5)$$

where  $\Delta N_{\text{ft}}^+(t)$  is the PCFT density after annealing time  $t$ ,  $\Delta N_{\text{ft}}^+(0)$  is the PCFT density at the beginning of annealing, i.e. at  $t = 0$ , and  $\tau^+ = 1/k^+$  is the time constant showing the annealing rate.

The behaviour of NCFT density ( $\Delta N_{\text{ft}}^-$ ) during the isothermal annealing could be more complex. In [21] two possible scenarios were discussed. According to the first scenario, PCFTs have been annealed by tunnelling electrons, but NCFTs have not ( $\Delta N_{\text{ft}}^- = \text{const}$ ). After some time, PCFTs are annealed, but NCFTs remain, turning  $\Delta N_{\text{ft}}$  negative. During modelling, the constant  $\Delta N_{\text{ft}}^-$  value, which is negative, should be added to equation (5).

According to the second scenario, which is more probable [21], the PCFTs are annealed, but NCFTs are created by the electrons that tunnel from the substrate under internal positive electric field and high temperature. In that way,  $\Delta N_{\text{ft}}^+(t)$  decreases, but  $\Delta N_{\text{ft}}^-(t)$  increases, and the net effect is the negative value of  $\Delta N_{\text{ft}}(t)$ . The reaction for NCFT creation process is



where  $N_{\text{ft}}^{o(-)}$  denotes the NCFT precursor,  $k^-$  is the reaction rate constant, and  $N_{\text{ft}}^-$  denotes the NCFT.

Reaction (6) gives the equation [21]:

$$\Delta N_{\text{ft}}^-(t) = \Delta N_{\text{ft}}^{\infty(-)} \left(1 - e^{-t/\tau^-}\right), \quad (7)$$

where  $\Delta N_{\text{ft}}^-(t)$  is the NCFT density after annealing time  $t$ ,  $\Delta N_{\text{ft}}^{\infty(-)}$  is the NCFT density after long annealing time ( $t \rightarrow \infty$ ) that is negative ( $\Delta N_{\text{ft}}^{\infty(-)} < 0$ ; see figures 5 and 6), and  $\tau^- = 1/k^-$  is the time constant showing the annealing rate.  $\Delta N_{\text{ft}}^-(t)$  at the beginning of annealing, i.e. at  $t = 0$ , equals zero ( $\Delta N_{\text{ft}}^-(0) = 0$ ).

The third scenario could also be included: both the PCFTs and NCFTs are annealed during isothermal annealing, but the annealing of PCFs is more intensive than annealing of NCFTs,

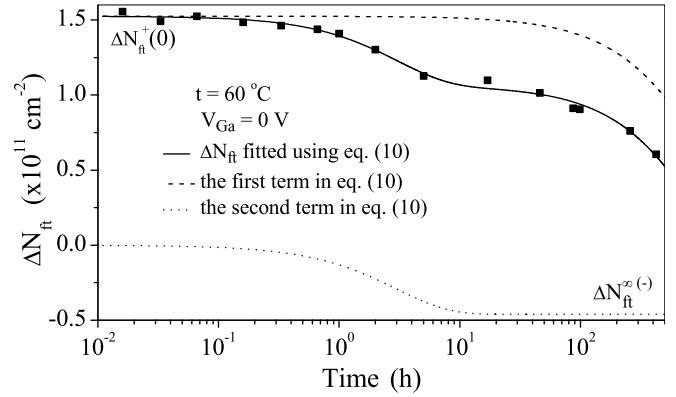


**Figure 5.** Modelling of isothermal annealing at  $t = 60^\circ\text{C}$  using equation (10). Both terms are shown.

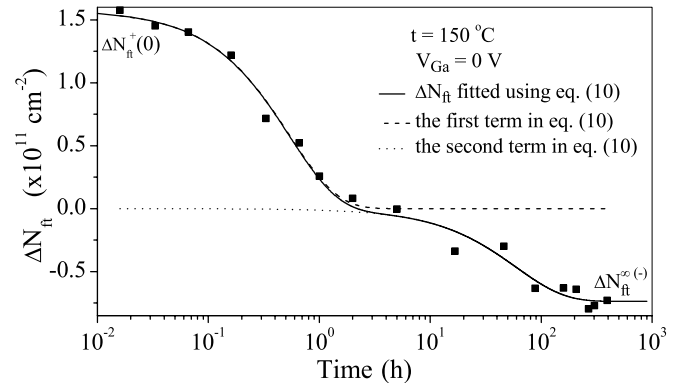
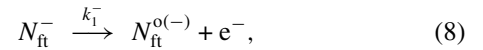


**Figure 6.** Modelling of isothermal annealing at  $t = 150^\circ\text{C}$  using equation (10). Both terms are shown.

and a net effect is a negative  $\Delta N_{\text{ft}}(t)$ . Namely, the electrons leave the NCFTs, turning the NCFTs in neutral FTs:



where  $N_{\text{ft}}^{o(-)}$  denotes annealed NCFT (similarly to equation (3)). The annealing equation for this process is

$$\Delta N_{\text{ft}}^-(t) = \Delta N_{\text{ft}}^-(0) \cdot e^{-t/\tau_1^-}. \quad (9)$$

where  $\Delta N_{\text{ft}}^-(t)$  is the NCFT density after annealing time  $t$ ,  $\Delta N_{\text{ft}}^-(0)$  is the NCFT density at the beginning of annealing, i.e. at  $t = 0$ , and  $\tau_1^- = 1/k_1^-$  is the time constant showing the annealing rate.

We have modelled all three scenarios. For the first scenario,  $\Delta N_{\text{ft}}^-$ , for the second, equation (7), and for third scenario, equation (9), should be added to equation (5). The results have shown that the second scenario gives the best modelling of experimental data. On the basis of this conclusion, the equation for the total FT density during isothermal annealing is obtained [21]:

$$\begin{aligned} \Delta N_{\text{ft}}(t) &= \Delta N_{\text{ft}}^+(t) + \Delta N_{\text{ft}}^-(t) \\ &= \Delta N_{\text{ft}}^+(0) \cdot e^{-t/\tau^+} + \Delta N_{\text{ft}}^{\infty(-)} \left(1 - e^{-t/\tau^-}\right). \end{aligned} \quad (10)$$

$\tau^+$  and  $\tau^-$  are the time constants showing the annealing rates, and they are connected with the rate constants  $k^+$  and

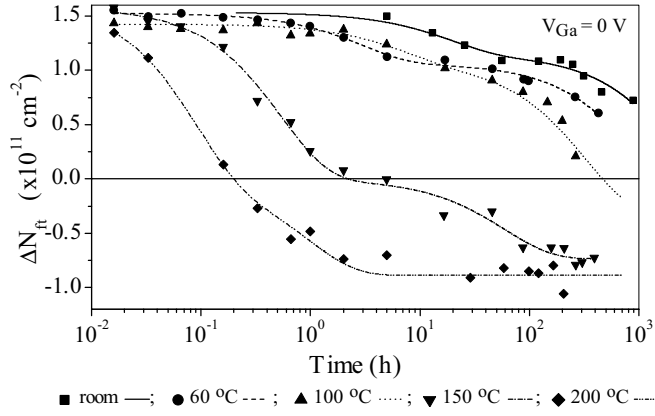


**Figure 7.** Modelling of isothermal annealing using equation (10).

$k^-$ :  $\tau^+ = 1/k^+$  and  $\tau^- = 1/k^-$ . The PCFTs are annealed, but NFCTs are formed during annealing by the electrons tunnelling from the substrate. The density of PCFT decreases, but density of NCFT increases, and the final effect is the negative value of  $\Delta N_{\text{fit}}$  [21].

Figures 5 and 6 show the results of  $\Delta N_{\text{fit}}$  modelling during isothermal annealing at  $t = 60$  and  $150^\circ\text{C}$  using equation (10). Both terms and their contributions to  $\Delta N_{\text{fit}}(t)$  are displayed. Figure 5 shows that all PCFTs have not been annealed, meaning either the annealing time was not long enough, or PCFTs contain more than one defect type (equation (7) assumes only one PCFT defect type). Looking at figure 6, it could be concluded that only one PCFT type exists, and all traps have been annealed after a few hours. However, our detailed analysis has shown that this conclusion is not valid, and at least one additional PCFT type exists in this case of  $150^\circ\text{C}$  (see the following text).

Figure 7 shows the modelling of  $\Delta N_{\text{fit}}$  during isothermal annealing at all investigated temperatures using equation (10). It could be seen that obtained modelling curves fit the experimental data very well.

Rate constants  $k^+$  and  $k^-$ , as well as the time constants  $\tau^+$  and  $\tau^-$  are connected with the activation energies  $E_a^+$  and  $E_a^-$  of PCFTs and NCFTs, respectively, by the Arrhenius equations:

$$k^+ = k_o^+ \cdot \exp(-E_a^+/k_B T) \Rightarrow \tau^+ \equiv 1/k^+ = \tau_o^+ \cdot \exp(E_a^+/k_B T), \quad (11)$$

$$k^- = k_o^- \cdot \exp(-E_a^-/k_B T) \Rightarrow \tau^- \equiv 1/k^- = \tau_o^- \cdot \exp(E_a^-/k_B T), \quad (12)$$

where  $\tau_o^+ = 1/k_o^+$ ,  $\tau_o^- = 1/k_o^-$ ,  $k_B = 1.38 \times 10^{-23} \text{ J K}^{-1}$  is the Boltzmann constant, and  $T$  is the absolute annealing temperature in  $K$ .  $k_o^+$  and  $k_o^-$  are known as the frequency factors (escape frequencies). Equations (11) and (12) assume that there is one type of PCFTs and one type of NCFTs, i.e. PCFTs and NCFTs have unique activation energies  $E_a^+$  and  $E_a^-$ , respectively.

The activation energies  $E_a^+$  and  $E_a^-$  could be obtained using the natural logarithms of equations (11),  $\ln \tau^+ = \ln \tau_o^+ + (E_a^+/k_B) 1/T$ , and (12),  $\ln \tau^- = \ln \tau_o^- + (E_a^-/k_B) 1/T$ , and the graph representing  $\ln \tau$  versus  $1/T$ , which is linear.  $\tau^+$  and  $\tau^-$  are found by the fittings shown in figure 7 using equation (10).

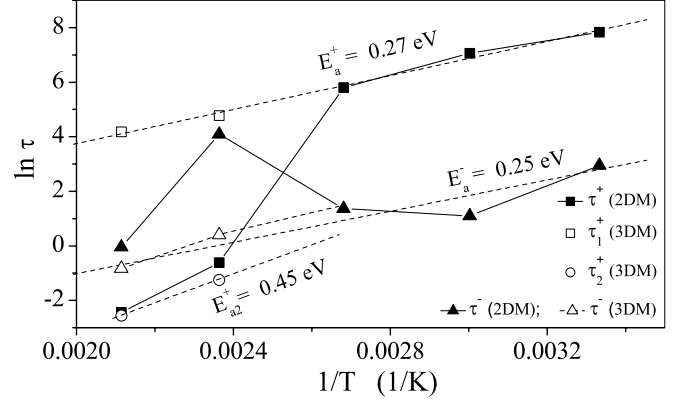
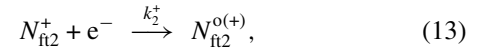


**Figure 8.** The activation energy determination.

Figure 8 shows the dependences of natural logarithms of time constants  $\tau^+$  and  $\tau^-$  on the reciprocal annealing temperatures. The  $\ln \tau^+$  values for the first three temperatures (room, 60 and  $100^\circ\text{C}$ ) satisfy a linear dependence, giving the activation energy of  $E_a^+ = 0.27 \text{ eV}$ , but for the highest temperatures of 150 and  $200^\circ\text{C}$  these values are out of straight line (the first two solid square symbol in figure 8). The  $\ln \tau^-$  for the first three temperatures also shows the linear dependence, giving the activation energy of  $E_a^- = 0.25 \text{ eV}$ , but  $\ln \tau^-$  values are out of this dependence for 150 and  $200^\circ\text{C}$  (the first two solid triangle symbols in figure 8).

**3.1.2. Three-defect model (3DM).** Deviation of  $\tau^+$  and  $\tau^-$  from the straight lines for 150 and  $200^\circ\text{C}$  indicates that the another trap(s) exist(s) at these temperature. We introduced one additional PCFT  $N_{\text{fit}}^+$  satisfying a reaction similar to reaction (3):



We modified equation (10) adding a term that corresponds to a new PCFT type from reaction (13):

$$\begin{aligned} \Delta N_{\text{fit}}(t) &= \Delta N_{\text{fit}}^+(t) + \Delta N_{\text{fit}}^-(t) \\ &= \Delta N_{\text{fit}1}^+(0) \cdot e^{-t/\tau_1^+} + \Delta N_{\text{fit}2}^+(0) \cdot e^{-t/\tau_2^+} \\ &\quad + \Delta N_{\text{fit}}^{o(-)} \left(1 - e^{-t/\tau^-}\right). \end{aligned} \quad (14)$$

where  $\tau_1^+$  and  $\tau_2^+$  are now the time constants for annealing of two PCFT types shown in the reactions (3) and (13), respectively. Otherwise,  $\Delta N_{\text{fit}}(0) = \Delta N_{\text{fit}1}^+(0) + \Delta N_{\text{fit}2}^+(0)$ , while  $\Delta N_{\text{fit}}^+(0) = \Delta N_{\text{fit}1}^+(0) + \Delta N_{\text{fit}2}^+(0)$  and  $\Delta N_{\text{fit}}^-(0) = 0$  (see figure 9).

The  $\tau_1^+$  values for  $t = 150$  and  $200^\circ\text{C}$  (open square symbols in figure 8), obtained by the modelling of  $\Delta N_{\text{fit}}(t)$  using equation (14), also satisfy the linear dependence in figure 8. The  $\tau_2^+$  values for these two temperatures are also shown, giving the higher activation energy of  $E_{a2}^+ = 0.45 \text{ eV}$ . All time constants are shown in table 1.

In figure 8, the  $\ln \tau^-$  obtained by the 2DM for all temperatures are shown using solid triangles, but by the 3DM for  $t = 150$  and  $200^\circ\text{C}$  using open triangles. The 3DM shows better linear dependence for the highest temperatures than 2DM. The linear fit gives the activation energy for NCFTs

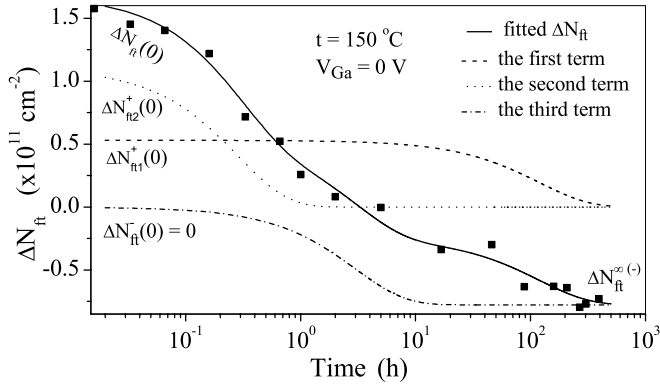


**Figure 9.** Modelling of isothermal annealing at  $t = 150\text{ }^\circ\text{C}$  using equation (14). All three terms are also shown.

**Table 1.** Time constants of different processes.

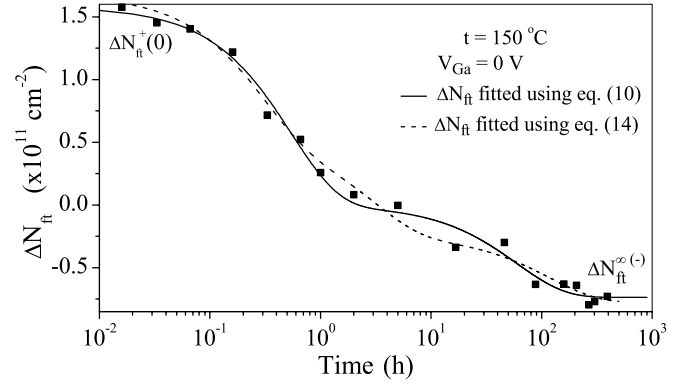
$t$ ( $^\circ\text{C}$ )	$\tau^+$ (h)	$\tau^-$ (h)	$\tau_1^+$ (h)	$\tau_2^+$ (h)
Room	2512.55	18.98	—	—
60	1162.59	2.989	—	—
100	331.09	3.91	—	—
150	0.54	1.55	118.95	0.285
200	0.087	0.435	64.87	0.0775

of  $E_a^- = 0.25\text{ eV}$ . The points for room temperature, 60 and  $100\text{ }^\circ\text{C}$  are obtained by 2DM (equation (10)), but for  $t = 150$  and  $200\text{ }^\circ\text{C}$  by 3DM (equation (14)). It is obvious that  $E_{al}^+ \approx E_a^-$ .

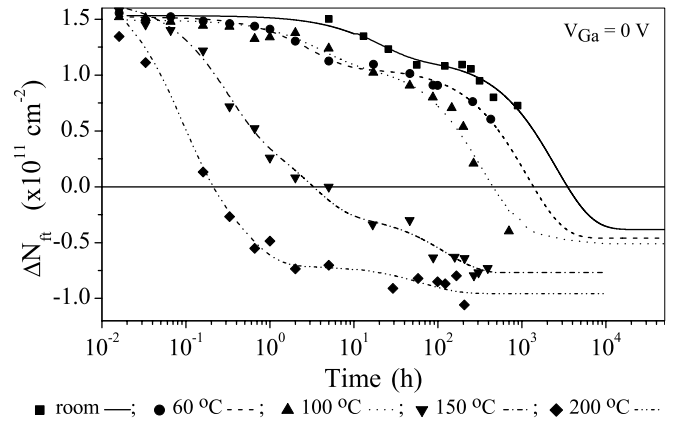
Alternatively, the activation energy could be found, in addition to using the time constants as in figure 8, either by the time to saturation of  $\Delta N_{ft}$ :  $t_{sat} = t_{sat,0} \cdot \exp(E_a/(k_B T))$  or by half time to the saturation:  $t_{1/2} = t_{1/2,0} \cdot \exp(E_a/(k_B T))$  [32]. The fourth, and most complicated method, is to use the model given in [16]. This model needs a frequency factor that is not known, and usually cannot be easily determined, but influences the activation energy value (see the next section). All methods have to give the same activation energy.

Figure 9, similarly to figure 6, shows the  $\Delta N_{ft}$  modelling during isothermal annealing at  $t = 150\text{ }^\circ\text{C}$ , but using equation (14) (all three terms are displayed; time constants are from table 1), and figure 10 using equations (10) and (14). As expected, equation (14) gives better fit, but the differences are not significant. Figures 11 and 12 display the results of isothermal annealing modelling using equation (14) up to saturation for 300/50 and 690/15 types, respectively, showing a possibility of FT behaviour predictions for longer isothermal annealing periods.

The gate oxide ( $\text{SiO}_2$ ) structure and the defects possibly created by radiation will be considered. A bond between a silicon and an oxygen in Si–O bond in the gate oxide is covalent, where ‘-’ represents two electrons making a covalent bond ( $\text{Si}\cdot\text{O}$ , where  $\cdot$  denotes an electron). A distance  $d$  between Si and O in Si–O bond varies from 0.152 to 0.169 nm and an angle  $\theta$  in the Si–O–Si bond varies from  $120$  and  $180^\circ$ , but the distance and angle are  $d = 0.162\text{ nm}$  and  $\theta = 140^\circ$ , respectively, in the case of non-strained silicon–oxygen bonds [33].



**Figure 10.** Modelling of isothermal annealing at  $t = 150\text{ }^\circ\text{C}$  using equations (10) and (14).



**Figure 11.** Modelling of isothermal annealing up to saturation using equation (14) for 300/50 transistor type.

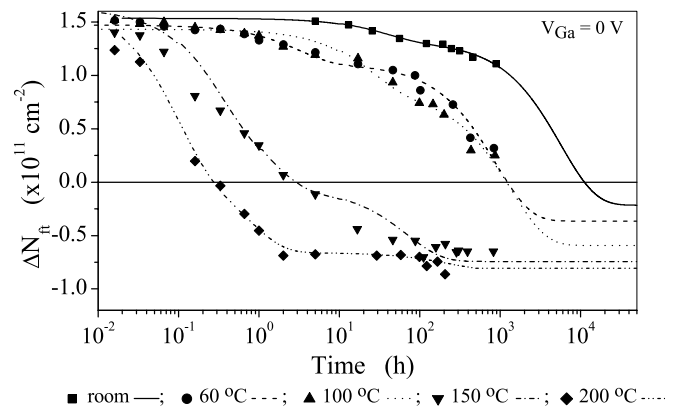


**Figure 12.** Modelling of isothermal annealing up to saturation using equation (14) for 690/15 transistor type.

During irradiation, the gamma photons interact with the electrons bound in the  $\text{SiO}_2$  molecule via Compton scattering, releasing the electrons and holes [29]. The released electrons are highly energetic and may be recombined with the holes at the place of production, or, which is more probable, may escape a recombination. The electrons that escape a recombination travel some distance until they leave the oxide, losing their kinetic energy through the collisions with other free electrons, or, what is the more probable, with the bonded electrons in  $\text{Si}_o\text{--O}$  and  $\text{Si}_o\text{--Si}_o$  covalent bonds in the oxide, releasing

more electrons, known as secondary electrons (the latter bond represents an oxygen vacancy, but ‘o’ denotes the oxide). Each secondary electron, before it has left oxide or being recombined by hole, can break a lot of covalent bonds in the oxide, producing a lot of new secondary highly energetic electrons, since its energy is usually much higher than an impact ionizing process energy. The electrons leaving the producing place escape the oxide very fast (for several picoseconds), but the holes remain in the oxide.

The holes released in the oxide bulk are usually only temporary, but not permanently trapped at the place of production, since there are no energetically deeper centres in the oxide bulk. The holes move towards one of interfaces (SiO<sub>2</sub>/Si or gate/SiO<sub>2</sub>), depending on the oxide electric field direction, where they have been trapped at energetically deeper trap hole centres: the strained silicon–oxygen bonds ( $\equiv \text{Si}_o - \text{O} - \text{Si}_o \equiv$ ), and the strained oxygen vacancy bonds  $\equiv \text{Si}_o - \text{Si}_o \equiv$ , both distributed near the interfaces.

The holes break the strained silicon–oxygen bonds, creating the amphoteric NBO centres ( $\equiv \text{Si}_o - \text{O}^{\cdot}$ ) and E<sub>s</sub><sup>′</sup> centres ( $^+ \text{Si}_o \equiv$ ), and the strained oxygen vacancy bonds creating E<sub>v</sub><sup>′</sup> centres ( $\equiv \text{Si}_o^+ \cdot \text{Si}_o \equiv$ ) [27]. It could be assumed that the strained silicon–oxygen bonds, and oxygen vacancies represent the main defect precursors of the positively charged FTs in the oxide bulk, near the interfaces. In addition to the defect creations by bond breaking, the mechanism of defects charging also exists. An NBO centre is an amphoteric defect that could be more easily charged negatively than positively by trapping an electron. Obviously, an NBO centre, as an energetically deeper centre, is the main precursor of the NCFTs in the interface regions of oxide bulk [27].

As has been said, the E<sub>v</sub><sup>′</sup> and E<sub>s</sub><sup>′</sup> centres, as well as the NBO centres, as the main radiation defects, represent energetically deeper hole and electron trapping centres, respectively. It should be noted that the energetic levels of one defect type can be various, i.e. chemically the same defects show different behaviours depending on the whole bond structure: the angles and distances between the surrounding atoms [27]. It could be an explanation for different defect behaviours at higher temperatures, in 2DM and 3DM, i.e. structurally the same defects show various behaviours depending on the angles and distances between host Si atom and adjacent atoms.

### 3.2. Isochronal annealing

The isochronal annealing represents the temperature increase in the constant temperature steps ( $\Delta T$ ) with the constant time intervals ( $\Delta t$ ) at each temperature (see figure 1(b)). The temperature steps were  $\Delta T = 10$  K, the transistors were kept at each temperature for time interval of  $\Delta t = 10$  min, and gate bias was  $V_{\text{Ga}} = 0$  V.

Figures 13 and 14 show the  $\Delta N_{\text{ft}}$  and  $\Delta N_{\text{st}}$  during isochronal annealing of 300/15 and 690/15 RADFETs, respectively.  $\Delta N_{\text{st}}$  initially increases slightly, then decreases, but  $\Delta N_{\text{ft}}$  continuously decreases (the same behaviour has been observed for the other RADFET types [21]).

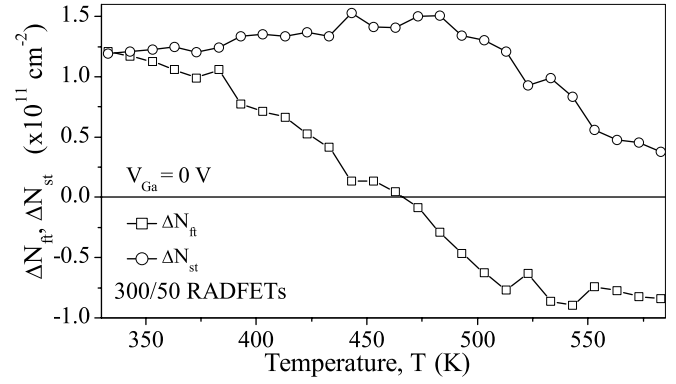


Figure 13. Isochronal annealing of 300/50 RADFETs.

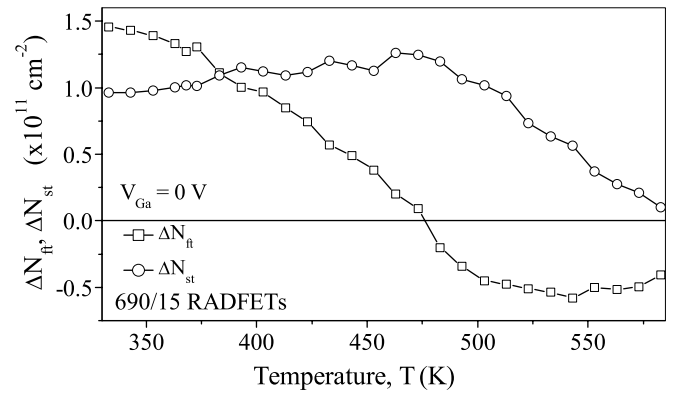


Figure 14. Isochronal annealing of 690/15 RADFETs.

The ‘unannealed’ fraction of fixed trapped charge, after temperature  $T$ ,  $N_{\text{ft}}(T)$ , is [16]

$$N_{\text{ft}}(T) = \frac{\Delta N_{\text{ft}}(T)}{\Delta N_{\text{ft}}(0)}, \quad (15)$$

where  $\Delta N_{\text{ft}}(0)$  is the FT density at the beginning of annealing, i.e. after irradiation, and  $\Delta N_{\text{ft}}(T)$  at the temperature  $T$  during isochronal annealing.

The  $N_{\text{ft}}$ , calculated by equation (15), for our case has the shape of logistic curve, and the following semi-empirical equation could be used [21]:

$$N_{\text{ft}}(T) = N_{\text{ft}}^+(T) + N_{\text{ft}}^-(T) = \frac{a_1}{1 + e^{b_1(T-c_1)}} + \frac{a_2}{1 + e^{b_2(T-c_2)}}, \quad (16)$$

which has two terms, the first, unannealed fraction of PCFTs,  $N_{\text{ft}}^+(T)$ , and the second, unannealed fraction of NCFTs,  $N_{\text{ft}}^-(T)$ .  $a_1$ ,  $b_1$ ,  $c_1$ ,  $a_2$ ,  $b_2$  and  $c_2$  are the fitting constants. The contributions of PCFTs and NCFTs to  $N_{\text{ft}}(T)$  were fitted simultaneously.

The fitting of unannealed fractions by equation (16) has shown that the second term is constant (see figures 15 and 16). Because of that, equation (16) was reduced to

$$N_{\text{ft}}(T) = \frac{a_1}{1 + e^{b_1(T-c_1)}} + a_2. \quad (17)$$

It has been shown by equation (7) that the NCFTs are created during isothermal annealing, but now it is concluded that

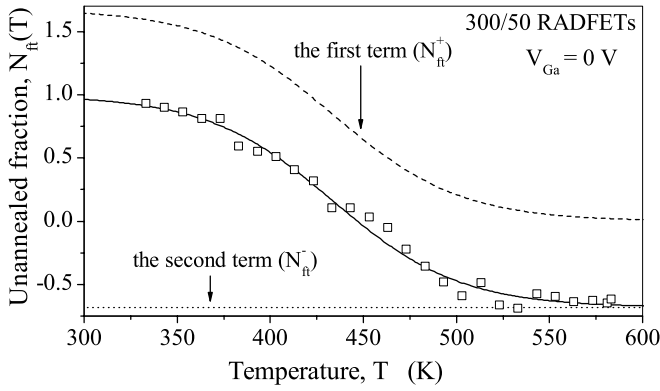


**Figure 15.** Unannealed fraction  $N_{fit}$  versus  $T$  of 300/50 RADFETs.

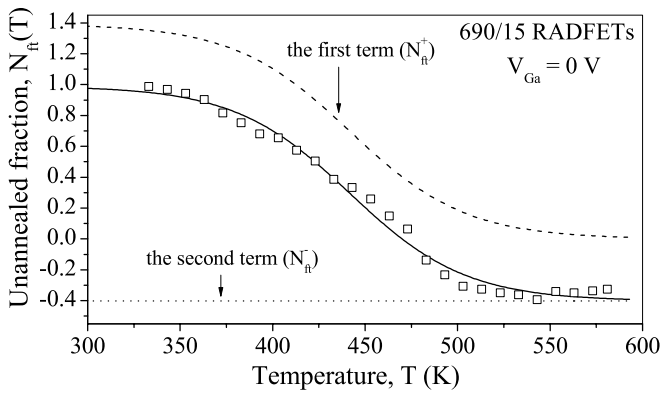


**Figure 16.** Unannealed fraction  $N_{fit}$  versus  $T$  of 690/15 RADFETs.

NCFTs are not changed during the isochronal annealing. Although it sounds controversial, looking at figures 5, 6 and 9 it could be easily concluded that the NCFT creations start at much longer annealing times than isochronal annealing time of  $\Delta t = 10$  min at a given temperature. Namely, during isochronal annealing the RADFETs were isothermally annealed for only  $\Delta t$  at  $T$ , then cooled to room temperature, and characterized (see figure 1(b)).

Figures 15 and 16 show the  $N_{fit}(T)$  fitted by equation (17) with the fitting constants:  $a_1 = 1.676$ ,  $b_1 = 0.02947 \text{ K}^{-1}$ ,  $c_1 = 434 \text{ K}$  and  $a_2 = -0.682$ , for 300/50 RADFETs, and  $a_1 = 1.393$ ,  $b_1 = 0.03198 \text{ K}^{-1}$ ,  $c_1 = 442 \text{ K}$ , and  $a_2 = -0.402$  for 690/15 RADFETs. The dashed line is for positive, and the dotted line for negative contribution. The full line represents the sum of these two contributions.

The first derivative of  $N_{fit}(T)$ ,

$$N'_{fit}(T) = \frac{dN_{fit}(T)}{dT}, \quad (18)$$

shows the rate of  $N_{fit}(T)$  annealing. Since, in our case,  $N_{fit}^- = a_2 = \text{const}$ , then  $N'_{fit}(T)$  is equal to the first derivative of function  $N_{fit}^+(T)$  (equation (17)):  $N'_{fit}(T) \equiv N_{fit}^{+'}(T) = dN_{fit}^+(T)/dT$ .  $c_1 = T^*$  represents the characteristic temperature for which the  $N_{fit}^+(T)$  and  $N_{fit}^{+'}(T)$  are maximal.

Figures 17 and 18 show the first term in equation (17),  $N_{fit}^+$  (left axis) and  $N_{fit}^{+'}$  (right axis) versus absolute temperature,  $T$ . Else, for  $T = T^*$  the first term in equation (17) always gives  $N_{fit}^+(T^*) \approx 0.5N_{fit}^+(0)$ . A peak of  $N_{fit}^{+'}$  (and  $N_{fit}^+$ ) for  $T^* \approx 434 \text{ K}$

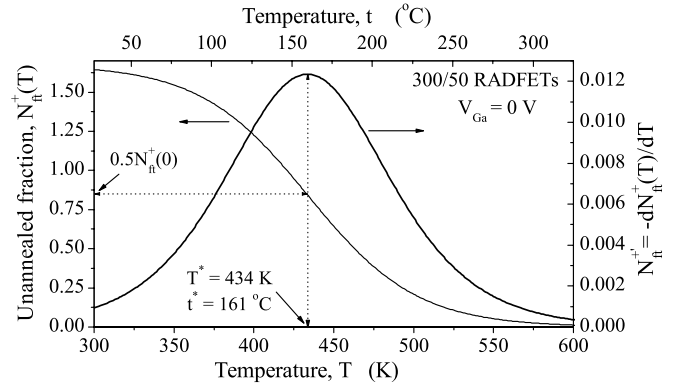


**Figure 17.**  $N_{fit}^+$  and  $N_{fit}^{+'}$  of 300/50 RADFETs.

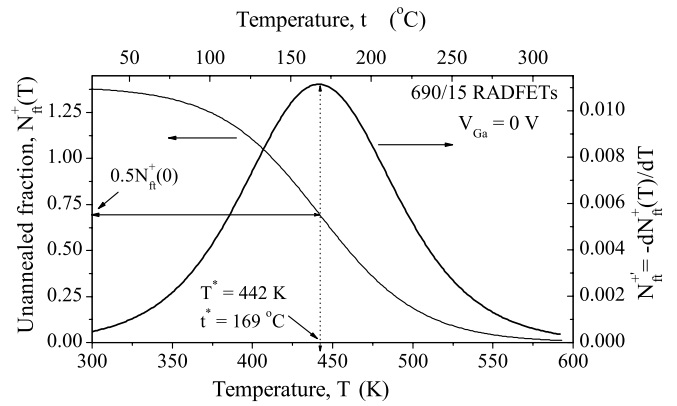


**Figure 18.**  $N_{fit}^+$  and  $N_{fit}^{+'}$  of 690/15 RADFETs.

(300/50 devices) and  $T^* \approx 442 \text{ K}$  (690/15 devices) could be seen. The peak height depends on the  $N_{fit}(T)$  curve slope. A slope is steeper ( $b_1$  is greater), a peak height is larger and a  $N_{fit}^+$  curve is sharper.

### 3.2.1. Activation energy analysis.

*What can we obtain from isochronal annealing?*

The trap distribution  $n_0(E_a)$  in activation energy  $E_a$  could be obtained from the isochronal annealing by the model [16, 17]. In that model, each isochronal temperature has its own  $E_a$  value [16]:

$$\frac{E_a}{k_B T} + \ln \left( \frac{E_a}{k_B T} + 2 \right) = \ln(A \cdot c \cdot T). \quad (19)$$

However,  $E_a$  in (19) depends on a frequency factor  $A$  that could not be uniquely found. If  $A$  increases 100 times, then  $E_a$  increases about 1.2 times, i.e. by 20% (see figure 14 in [32]). Although this difference does not seem so strong, the  $A$  value range that has been used is significantly wider (from  $A = 10^7$  to  $10^{13} \text{ s}^{-1}$  [16–32, 34]), and the difference in  $E_a$  calculated for  $A = 10^7 \text{ s}^{-1}$  and  $10^{13} \text{ s}^{-1}$  is even 64%. Because of that, it may be better to show  $N_{fit}$  and  $N_{fit}^+ = dN_{fit}(T)/dT$  versus  $T$ , and not calculate  $E_a$  using equation (19).

*What does the isochronal curve really give?*

The isochronal curve representing the dependence of unannealed fraction  $N_{fit}$  on isochronal temperature  $T$  shows

how many defects have remained after the isothermal annealing of duration  $\Delta t$  at temperature  $T$ . The better indicator is the first derivative of  $N_{\text{ft}}(T)$ ,  $N'_{\text{ft}}(T)$  (equation (18)), that shows how many defects have been annealed during  $\Delta t$  at  $T$  (figure 1).

$N'_{\text{ft}}(T)$  shows the annealed defect fraction,  $n_o$ , that has been annealed during  $\Delta t$  at  $T$ . i.e. the dependence of  $n_o$  on  $T$ , rather than on  $E_a$  [35]:

$$N'_{\text{ft}}(T) \approx \frac{N_{\text{ft}}(T) - N_{\text{ft}}(T - \Delta T)}{\Delta T} \sim n_o(T). \quad (20)$$

Actually, in our case,  $N'_{\text{ft}}(T)$  shows the rate of PCFT annealing for the time interval  $\Delta t$  at  $T$ .

For a unique mechanism, i.e. unique trap type,  $E_a$  is temperature independent. Here, only the PCFT annealing is considered, since NCFT density is constant during isochronal annealing (see figures 15 and 16). During an isochronal annealing, several defect types of PCFTs, with unannealed fractions  $N_{\text{ft1}}^+(T)$ ,  $N_{\text{ft2}}^+(T)$ ,  $N_{\text{ft3}}^+(T)$ , ..., having their own activation energies  $E_{a1}^+$ ,  $E_{a2}^+$ ,  $E_{a3}^+$ , ..., and their own time constants  $\tau_1^+(T)$ ,  $\tau_2^+(T)$ ,  $\tau_3^+(T)$ , ..., that show annealing rates, could be active. Otherwise, the following must be valid for the unannealed fraction of PCFTs:  $N_{\text{ft}}^+(T) = N_{\text{ft1}}^+(T) + N_{\text{ft2}}^+(T) + N_{\text{ft3}}^+(T) + \dots$ . The values of activation energies and time constants have to be in relation to the values obtained by isothermal annealing.

For a trap (defect) type with  $E_{a1}^+$ , the dependence of time constant  $\tau_1^+$  on  $T$  is (equation (11))

$$\tau_1^+(T) = \tau_{o1}^+ \cdot e^{E_{a1}^+/(k_B T)}. \quad (21)$$

As long as  $\ln \tau_1^+(T)$  is linear with  $1/T$ :

$$\ln \tau_1^+(T) = \ln \tau_{o1}^+ + (E_{a1}^+/k_B) 1/T, \quad (22)$$

one trap type of PCFTs is active, i.e. there is a unique activation energy  $E_{a1}^+$ . It means that each isochronal temperature step does not have its own  $E_a$  value, but one  $E_a$  value is valid for more temperature steps.

It should be started from a temperature for which it could be proposed that only one defect type is active (e.g. from room temperature  $T \approx 300$  K) up to a temperature for which  $\ln \tau_1^+(T)$  is still linear with  $1/T$ .

How could  $\tau_1^+(T)$  be found? The reaction (3) corresponding to neutralization/compensation of one PCFT type during annealing by the tunnelling electrons could be used for the isochronal annealing, since  $T = \text{const}$  during  $\Delta t$  (figure 1(b)).

On the basis of equation (5), the decrease in unannealed fraction of the active PCFT type,  $N_{\text{ft1}}^+(T)$ , during the  $\Delta t$  time interval at temperature  $T$  is

$$N_{\text{ft1}}^+(T) = N_{\text{ft1}}^+(T - \Delta T) \cdot e^{-\Delta t/\tau_1^+(T)}, \quad (23)$$

where  $N_{\text{ft1}}^+(T - \Delta T)$  is the unannealed fraction at the temperature  $(T - \Delta T)$ , i.e. at the beginning of the  $\Delta t$  interval at the temperature  $T$ , and  $N_{\text{ft1}}^+(T)$  is at the end of this interval. From equation (23),  $\tau_1^+(T)$  during isothermal annealing of  $\Delta t$  duration at  $T$  is

$$\tau_1^+(T) = \frac{\Delta t}{\ln(N_{\text{ft1}}^+(T - \Delta T)/N_{\text{ft1}}^+(T))}. \quad (24)$$

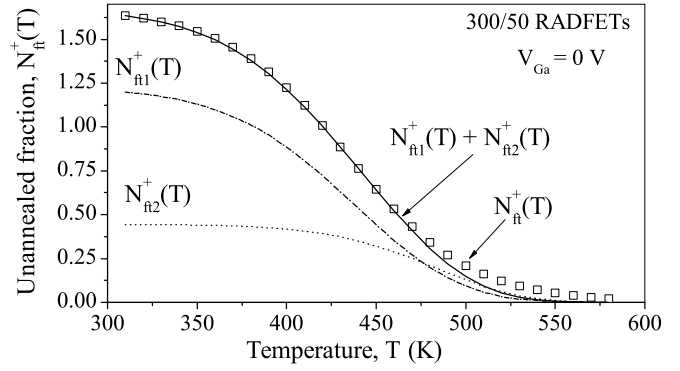


Figure 19. The modelling of unannealed fraction  $N_{\text{ft}}^+$ .

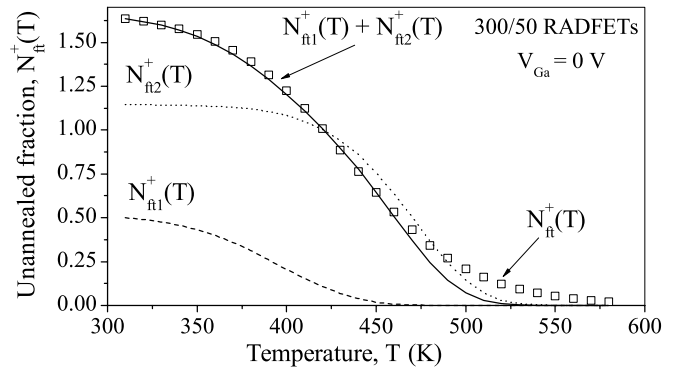


Figure 20. The modelling of unannealed fraction  $N_{\text{ft}}^+$ .

In the simplest case, only one PCFT type is active, which is responsible for the whole isochronal annealing, meaning  $N_{\text{ft}}^+(T) = N_{\text{ft1}}^+(T)$ . However, in real cases, more PCFT types are usually active and the knowing of starting  $N_{\text{ft1}}^+(T - \Delta T)$  value is a problem (see figures 19 and 20). If a starting value  $N_{\text{ft1}}^+(T - \Delta T)$  were known, then  $N_{\text{ft1}}^+(T)$  would be calculated from  $N_{\text{ft1}}^+(T - \Delta T) - N_{\text{ft1}}^+(T) = N_{\text{ft1}}^+(T - \Delta T) - N_{\text{ft1}}^+(T)$ .

In our case, the isochronal data modelling has shown that  $\ln \tau_1^+(T)$  is linear with  $1/T$  in the interval from  $T_1 = 300$  to  $T_2 = 380$  K ( $\approx 30$ – $100$  °C), meaning one type of PCFTs is active, and one  $E_a$  is valid in this temperature interval. The same results are obtained from isothermal annealing (see figure 8).

If one PCFT type cannot model the experimental data of  $N_{\text{ft}}^+(T)$  for all isochronal temperatures well, then additional PCFT type with time constant  $\tau_2^+$  and activation energy  $E_{a2}^+$  should be included, and so on.

In our case, the  $\tau_1^+(T)$  for temperatures higher than  $T_2 = 380$  K deviates from linear curve, and a new  $\tau_2^+(T)$  should be found, keeping the  $\ln \tau_1^+(T)$  linear with  $1/T$ . The procedure would be similar, but a problem is that the value of  $N_{\text{ft2}}^+(T_2)$ , which is not unique, is unknown.

A lot of combinations of starting values of  $N_{\text{ft}}^+(T)$  ( $N_{\text{ft1}}^+(0)$  and  $N_{\text{ft2}}^+(0)$ ) could well fit  $N_{\text{ft}}^+(T) (= N_{\text{ft1}}^+(T) + N_{\text{ft2}}^+(T))$ , i.e.  $N_{\text{ft1}}^+(0)$  and  $N_{\text{ft2}}^+(0)$  are not uniquely defined, representing a modelling problem. It could be seen in figures 19 and 20, showing two combinations of starting values, from a lot of possible combinations, which model well the PCFT unannealed fraction ( $N_{\text{ft}}^+$ ).

Discrepancy between modelled and calculated  $N_{\text{fi}}^+$  values for the temperatures higher than 470 K ( $\approx 200^\circ\text{C}$ ) means a new (the third) PCFT type should be included. It should be noted that the 3DM has also shown that two PCFT types could model the isothermal annealing up to  $200^\circ\text{C}$ .

#### 4. Conclusion

The isothermal and isochronal annealing of irradiated RADFETs has been performed. During the isothermal annealing (thermal annealing at a constant temperature), the PCFTs were annealed, but the behaviour of NCFTs could be more complex. Three models for NCFT behaviour explanations during isothermal annealing have been proposed. A model assuming that the NCFTs are created during isothermal annealing has given the best simulation of  $\Delta N_{\text{fi}}(t)$  with annealing time, comparing with the other two models: NCFTs are not changed and NCFTs are annealed during isothermal annealing.

Using the two-defect model (2DM), which assumes one defect type for PCFTs and another defect type for NCFTs, the  $\Delta N_{\text{fi}}$  during isothermal annealing has been successively modelled. However, the activation energies of PCFTs and NCFTs using 2DM could be calculated only for room temperature,  $t = 60$  and  $100^\circ\text{C}$ . For the temperatures of  $t = 150$  and  $200^\circ\text{C}$  a more complicated model containing three defects (called the three-defect model—3DM) had to be used. This model contains additional PCFT type, and could be used for the isothermal annealing prediction of irradiated RADFETs. Alternatively, using 3DM the activation energies for the whole temperature range could be calculated.

Two logistic functions have been initially used for the modelling of positive part, due to PCFTs, and negative part, due to NCFTs, of isochronal unannealed curve. However, the modelling has shown that the unannealed fraction of PCFT decreases, but that of NCFTs has not been changed during isochronal annealing. The first derivative of logistic function gives the characteristic temperature for which the annealing is maximal. Unfortunately, a procedure for activation energy determination by isochronal annealing is dependent on frequency factor that usually cannot be easily determined. Isothermal annealing is more time consuming, but the activation energy determination is parameter independent.

A good conformity in the results of defect modellings during isothermal and isochronal annealing has been obtained. Namely, both modellings have shown that one defect type of PCFTs is active up to  $100^\circ\text{C}$ , two defect types of PCFTs are active from  $100^\circ\text{C}$  up to  $200^\circ\text{C}$ , and additional defect(s) should be included for temperatures higher than  $200^\circ\text{C}$ . It could be concluded that less time consuming isochronal annealing is a very good tool for revealing defects created by various stress types, such as ionizing radiation, high field electric stress, charge injection and so on.

#### Acknowledgment

This work has been supported by the Ministry of Education and Science of the Republic of Serbia, under the project III43011,

and European Commission, under the project FP7 No 207 122 RADDOS.

#### References

- [1] Holmes-Siedle A and Adams L 1986 RADFET: a review of the use of metal–oxide–silicon devices as integrating dosimeters *Radiat. Phys. Chem.* **28** (2) 235–44
- [2] Tarr N G, Shortt K, Wang Y and Thomson I 2004 A sensitive, temperature-compensated, zero-bias floating gate MOSFET dosimeter *IEEE Trans. Nucl. Sci.* **NS-51** 1277–82
- [3] Lipovetzky J, Redin E G and Faigón A 2007 Electrically erasable metal–oxide–semiconductor dosimeters *IEEE Trans. Nucl. Sci.* **NS-54** 1244–50
- [4] Shamim A, Arsalan M, Roy L, Shams M and Tarr G 2008 Wireless dosimeter: system-on-chip versus system-in-package for biomedical and space applications *IEEE Trans. Circuits Sys.—II: Express Briefs* **55** 643–7
- [5] Stanić S, Asano Y, Ishino H, Igarashi A, Iwaida S, Nakano Y, Terazaki H, Tsuboyama T, Yoda I and Žontar D 2005 Radiation monitoring in Mrad range using radiation-sensing field-effect transistors *Nucl. Instrum. Methods Phys. Res. A* **545** 252–60
- [6] Ravotti F, Glaser M, Saigné F, Dusseau L and Sarabayrouse G 2006 Prediction of the thermal annealing of thick oxide metal–oxide–semiconductor dosimeters irradiated in a harsh radiation environment *Appl. Phys. Lett.* **89** 083503
- [7] Benson C, Albadri A, Joyce M J and Price R A 2006 The empirical dependence of radiation-induced charge neutralization on negative bias in dosimeters based on the metal–oxide–semiconductor field-effect transistor *J. Appl. Phys.* **100** 044505
- [8] Stanković S, Ilić R D, Davidović M, Kovačević M and Davidović D 2008 Influence of packaging configuration with kovar lid on RADFET response to proton irradiation *Nucl. Technol. Radiat. Protect.* **23** 37–40
- [9] Yilmaz E, Dogan I and Turan R 2008 Use of  $\text{Al}_2\text{O}_3$  layer as a dielectric in MOS based radiation sensors fabricated on a Si substrate *Nucl. Instrum. Methods Phys. Res. B* **266** 4896–8
- [10] Edgecock R, Matheson J, Weber M, Villani E G, Bose R, Khan A, Smith D R, Adil-Smith I and Gabrielli A 2009 Evaluation of commercial programmable floating gate devices as radiation dosimeters *J. Instrum.* **4** P02002
- [11] Rosenfeld A 2002 MOSFET dosimetry on modern radiation oncology modalities *Radiat. Prot. Dosim.* **101** 393–8
- [12] Ehringfeld C, Schmid S, Poljanc K, Kirisits C, Aiginger H and Georg D 2005 Application of commercial MOSFETs detectors for *in vivo* dosimetry in the therapeutic x-ray range from 80 kV to 250 kV *Phys. Med. Biol.* **50** 289–303
- [13] Asensio L J, Carvajal M A, Lopez-Villanueva J A, Vilches M, Lallena A M and Palma A J 2006 Evaluation of a low-cost commercial MOSFET as radiation dosimeter *Sensors Actuators A* **125** 288–95
- [14] Lavallee M-C, Gingras L and Beaulieu L 2006 Energy and integrated dose dependence of MOSFET dosimeter sensitivity for irradiation energies between 30 keV and  $^{60}\text{Co}$  *Med. Phys.* **33** 3683–9
- [15] Beyer G P, Mann G, Pursley J, Espenhahn E, Fraise C, Godfrey D, Oldham M, Carrea T, Bolick N and Scarantino C 2008 An implantable MOSFET dosimeter for the measurement of radiation dose in tissue during cancer therapy *IEEE Sensor J.* **8** 38–51
- [16] Danchenko V, Desai U D and Brashears S S 1968 Characteristics of thermal annealing of radiation damage in MOSFETs *J. Appl. Phys.* **39** 2417–24
- [17] Mallik A, Vasi J and Chandorkar A N 1993 The nature of the hole traps in reoxidized nitrided oxide gate dielectrics *J. Appl. Phys.* **74** 2665–8

- [18] Saigné F, Dusseau L, Albert L, Fesquet J, Gasiot J, David J P, Ecoffet R, Schrimpf R D and Galloway K F 1997 Experimental determination of the frequency factor of thermal annealing processes in metal-oxide semiconductor gate-oxide structures *J. Appl. Phys.* **82** 4102–7
- [19] Saigné F, Dusseau L, Fesquet J, Gasiot J, Ecoffet R, David J P, Schrimpf R D and Galloway K F 1997 Experimental validation of an accelerated method of oxide-trap-level characterization for predicting long term thermal effects in metal oxide semiconductor devices *IEEE Trans. Nucl. Sci.* **44** 2001–7
- [20] Dusseau L, Randolph T L, Schrimpf R D, Galloway K F, Saigné F, Fesquet J, Gasiot J and Ecoffet R 1997 Prediction of low dose-rate effects in power metal oxide semiconductor field effect transistors based on isochronal annealing measurements *J. Appl. Phys.* **81** 2437–41
- [21] Ristić G S 2009 Thermal and UV annealing of irradiated pMOS dosimetric transistors *J. Phys. D: Appl. Phys.* **42** 135101
- [22] Chabrerie C, Autran J, Paillet P, Flament O, Leray J and Boudenot J 1997 Isothermal and isochronal annealing temperature activated phenomena methodology to study post-irradiation *IEEE Trans. Nucl. Sci.* **NS-44** 2007–12
- [23] Flament O, Paillet P and Leray J 1999 Considerations on isochronal anneal technique: from measurement to physics *IEEE Trans. Nucl. Sci.* **NS-46** 1526–33
- [24] Saigné F, Dusseau L, Fesquet J, Gasiot J, Ecoffet R, Schrimpf R D and Galloway K F 2000 Prediction of the one-year thermal annealing of irradiated commercial devices based on experimental isochronal curves *IEEE Trans. Nucl. Sci.* **NS-47** 2244–8
- [25] Saigné F, Dusseau L, Fesquet J, Gasiot J, Ecoffet R, Schrimpf R D and Galloway K F 2001 Evaluation of MOS devices' total dose response using the isochronal annealing method *IEEE Trans. Nucl. Sci.* **48** 2170–3
- [26] Jaksic A, Ristic G, Pejovic M, Mohammadzadeh A, Sudre C and Lane W 2002 Gamma-ray irradiation and post-irradiation responses of high dose range RADFETs *IEEE Trans. Nucl. Sci.* **49** 1356–63
- [27] Ristić G S 2008 Influence of ionizing radiation and hot carrier injection on metal-oxide-semiconductor transistors *J. Phys. D: Appl. Phys.* **41** 023001 Topical Review
- [28] McWhorter P J and Winokur P S 1986 Simple technique for separating the effects of interface traps and trapped-oxide charge in metal-oxide-semiconductor transistors *Appl. Phys. Lett.* **48** 133–5
- [29] Ma T P and Dressendorfer P V 1989 *Ionizing Radiation Effects in MOS Devices and Circuits* (New York: Wiley)
- [30] Glasstone S 1946 *Textbook of Physical Chemistry* (Princeton, NJ: Van Nostrand-Reinhold)
- [31] Reed M L 1987 Si-SiO<sub>2</sub> interface trap anneal kinetics *PhD Thesis* Stanford University, Stanford
- [32] Ristić G S, Pejović M M and Jakšić A B 2000 Analysis of postirradiation annealing of n-channel power vertical double-diffused metal-oxide-semiconductor transistors *J. Appl. Phys.* **87** 3468–77
- [33] Helms R and Poindexter E H 1994 The silicon-silicon-dioxide system: its microstructure and imperfections *Rep. Prog. Phys.* **57** 791–852
- [34] Hwu J-G and Fu S-L 1989 Improvement in radiation hardness of oxide by successive irradiation-then-anneal treatments *Solid-State Electron.* **32** 615–21
- [35] Press W H, Flannery B P, Teukolsky S A and Vetterling W T 1986 *Numerical Recipes* (Cambridge: Cambridge University Press)